

NGC 7468: a galaxy with an inner polar disk

L.V. Shalyapina¹, A.V. Moiseev², V.A. Yakovleva¹, V.A. Hagen-Thorn¹, and O.Yu. Barsunova¹

¹ Astronomical Institute, St. Petersburg State University, Universitetsky pr.28, Petrodvorets, 198504 Russia

² Special Astrophysical Observatory, Russian Academy of Sciences, Nizhnii Arkhyz, Karachai-Cherkessian Republic, 357147 Russia

Received January 22, 2004

Abstract. We present our spectroscopic observations of the galaxy NGC 7468 performed at the 6-m Special Astrophysical Observatory telescope using the UAGS long-slit spectrograph, the multipupil fiber spectrograph MPFS, and the scanning Fabry-Perot interferometer (IFP). We found no significant deviations from the circular rotation of the galactic disk in the velocity field in the regions of brightness excess along the major axis of the galaxy (the putative polar ring). Thus, these features are either tidal structures or weakly developed spiral arms. However, we detected a gaseous disk at the center of the galaxy whose rotation plane is almost perpendicular to the plane of the galactic disk. The central collision of NGC 7468 with a gas-rich dwarf galaxy and their subsequent merging seem to be responsible for the formation of this disk.

INTRODUCTION

Whitmore et al. (1990) included NGC 7468 (Mrk 314) in their catalog of polar-ring galaxies (PRGs), candidate PRGs, and related objects as a probable candidate (C-69). The direct images (Fig. 1) of this galaxy show an extended low surface brightness base and a bright nuclear region resolvable into several individual condensations. Lobes are observed along the major axis on the galaxy's southern and northern sides, which may suggest the existence of a ring; this was the reason why NGC 7468 was included in the above catalog. The southern protrusion transforms into a faint bar that ends with a brightening whose distance from the galaxy's center in the plane of the sky is $\sim 45''$, or ~ 7 kpc. (For the line-of-sight velocity we found, $V_{gal} = 2220 \text{ km s}^{-1}$, and $H_0 = 65 \text{ km s}^{-1} \text{ Mpc}^{-1}$, the distance to the galaxy is 34 Mpc, which yields a scale of 0.16 kpc in $1''$).

NGC 7468 was initially classified as a peculiar elliptical galaxy (RC3, LEDA). However, according to a detailed photometric study by Evstigneева (2000), it should be considered to be a late-type spiral or an irregular galaxy. Indeed, the galaxy is rich in gas, as follows from neutral and molecular hydrogen data (Taylor et al. 1993, 1994; Richter et al. 1994; Wiklind et al. 1995). The ratios $M_{HI}/L_B = 0.621$ and $M_{H_2}/L_B = 0.06$ ($M_{H_2}/M_{HI} = 0.11$) derived for NGC 7468 are characteristic of galaxies of late morphological types (Young et al. 1989). The galaxy is an infrared source ($L_{IR}/L_B \sim 0.6$), suggesting the presence

of dust whose mass is estimated to be $0.4 \cdot 10^6 M_\odot$ (Huchtmeier et al. 1995).

In the central part of the galaxy, Petrosyan et al. (1979) distinguished three condensations whose emission spectra were studied by Petrosyan (1981) and subsequently by Nordgren et al. (1995). Since the spectra for the galaxy's central region are similar to those for H II regions, beginning with the works by Thuan et al. (1981), this object has been attributed to H II galaxies or blue compact dwarf galaxies (BCDGs) with active star formation in their central regions. The estimates of the star formation rate (Evstigneeva 2000; Cairo et al. 2001b) correspond to the star formation rate in BCDGs.

The velocity field inferred from neutral hydrogen (Taylor et al. 1993, 1994) exhibits no features in any of the two lobes and in the brightening region. These authors pointed out that the central isovelocity is distorted (oval distortion), which may be indicative of the presence of a bar. However, the spatial resolution of these observations is not high.

The photometry performed by Evstigneeva (2000) and Cairo et al. (2001b) show that the color of the northern and southern lobes and the brightening is bluer than that in the remaining regions of the galaxy (except for the nuclear region), which was considered by Evstigneeva (2000) as evidence for the presence of an outer polar ring around NGC 7468.

The initial assumption that the brightening to the south of the galaxy is a superassociation (Petrosyan 1981) was replaced by Evstigneeva (2000) with the suggestion that this is a companion galaxy, probably because galaxy

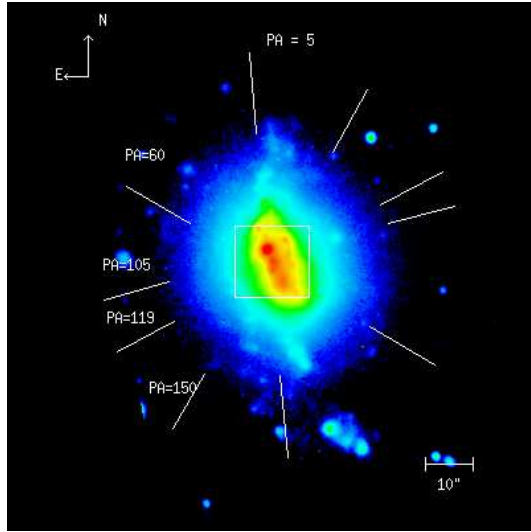


Fig. 1. Image of the galaxy NGC 7468 obtained with the 6 m telescope through a filter centered at $\lambda 6622\text{\AA}$; the UAGS slit locations and the MPFS field during observations are shown.

interaction is believed to be the most probable cause of the polar-ring formation and because she failed to find another suitable candidate that would confirm the interaction. Meanwhile, Taylor et al. (1993) pointed out that there is a faint galaxy 4'6 (45.5 kpc) north of NGC 7468 that the authors believe to be a possible companion of NGC 7468. The currently available information is clearly insufficient to determine whether NGC 7468 belongs to PRGs. The velocity field of the galaxy should be studied with a high spatial resolution. This paper presents the results of such a study based on optical spectroscopy.

OBSERVATIONS AND DATA REDUCTION

We performed our spectroscopic observations of the galaxy NGC 7468 at the prime focus of the 6-m Special Astrophysical Observatory (SAO) telescope with the long-slit spectrograph (UAGS), the multipupil fiber spectrograph (MPFS) (Afanasiev et al. 2001), and the scanning Fabry-Perot interferometer (IFP) (see Moiseev (2002) and the SAO WWW-site¹). The table 1 gives a log of observations.

The reduction technique that we used was described previously (Shalyapina et al. (2004)).

The long-slit spectra were taken near the H_α line (see the table 1). The H_α and $[\text{SII}]\lambda\lambda 6716, 6730\text{\AA}$ emission lines proved to be brightest in the spectra; in addition, the $[\text{NII}]\lambda\lambda 6548, 6583\text{\AA}$, $\text{HeI}\lambda 6678\text{\AA}$ lines were observed. The line-of-sight velocity curves were constructed from all lines. The accuracy of these measurements is $\pm 10\text{ km s}^{-1}$.

The central region of the galaxy was observed with the MPFS in the green spectral range. This range includes metal absorption lines ($\text{MgI}\lambda 5175\text{\AA}$, $\text{FeI}\lambda 5229\text{\AA}$, $\text{FeI+CaI}\lambda 5270\text{\AA}$, etc.) and the H_β and $[\text{OIII}]\lambda\lambda 4959, 5007\text{\AA}$ emis-

sion lines. Spectra from 240 spatial elements that form a 16×15 array in the plane of the sky were taken simultaneously.

Based on emission lines, we constructed the two dimensional maps of the intensity and line-of-sight velocity distributions (velocity fields). The line-of-sight velocities were determinations with accuracy of $10 - 15\text{ km s}^{-1}$. We used the spectra of the twilight sky and the galactic nucleus as templates for cross-correlation when constructing the velocity field for the stellar component. The errors in the line-of-sight velocities determined from absorption lines were found to be $\sim 15 - 20\text{ km s}^{-1}$.

Our IFP observations were performed near the H_α line. Premonochromatization was made using a filter with a central wavelength of 6578\AA and $FWHM = 19\text{\AA}$. The readout was made in 2×2 -pixel binning mode, with 512×512 -pixel images being obtained in each spectral channel. These data were used to construct the velocity field and the H_α and continuum brightness maps. The measurement errors of the line-of-sight velocities do not exceed 10 km s^{-1} .

RESULTS OF THE UAGS OBSERVATIONS AND THEIR ANALYSIS

The line-of-sight velocity curves constructed from different emission lines are similar. Figure 2 shows the data obtained from the H_α line at five locations of the UAGS slit. The point of maximum brightness that coincides with the southernmost of the three condensations was taken as zero. As we see from the figures, all line-of-sight velocity curves are peculiar. Let us consider these peculiarities in more detail.

The line-of-sight velocity curve obtained at a slit location close to the galaxy's major axis ($PA = 5^\circ$) is shown in Fig. 2a. In general, its shape agrees with that expected for the rotation of the galaxy's gaseous disk around its minor axis. In the region $-18'' \leq R \leq 20''$, the line-of-sight velocities change from 2140 km s^{-1} to 2030 km s^{-1} , flattening out at $R \geq 20''$. However, the change in the velocity is not monotonic. The waves that probably associated with individual HII regions are seen in the curve at $R \approx -3'' - 5''$ and $R \approx 12''$, and a step where the velocity is almost constant is noticeable at $0 \leq R \leq 7''$. Obviously, the gas responsible for the emission here is not involved in the rotation of the galaxy's main disk.

The presence of a kinematically decoupled gaseous subsystem at the center is confirmed by the line-of-sight velocity curves for position angles close to the minor axis ($PA = 105^\circ$, $PA = 119^\circ$). In both cases, a rectilinear segment with a gradient $dV/dR \approx 200\text{ km s}^{-1}\text{ kpc}^{-1}$ is clearly seen in the region $0 \leq R \leq 3''$, suggesting the rigid-body rotation of the gas around the galaxy's major axis. To the east of the center, the line-of-sight velocities are almost constant and, on average, equal to 2115 km s^{-1} . The emission here is attributable to the gas of the galaxy's disk that rotates around its minor axis. At $R \geq 3''$, the behavior of

¹ <http://www.sao.ru/hq/lsfvo/devices.html>

Table 1. Log of observations of NGC 7468

Instrument, date date	Exposure time, s	Field "	Scale, "/px	Spectral resolution, Å	Seeing "	Spectral region, Å	P.A. field
UAGS 2-4.10.99	1800	2x140	0.4	3.6	1.3	6200-7000	5°
	1200	2x140	0.4	3.6	1.5	6200-7000	60°
	1200	2x140	0.4	3.6	1.5	6200-7000	105°
	1800	2x140	0.4	3.6	1.3	6200-7000	150°
	300	2x140	0.4	3.6	1.3	6200-7000	119°
MPFS 08.12.01	1800	16x15	1	4.5	2.0	4600-6000	center
IFP 05.09.2002	32 × 180	5' × 5'	0.56	2.5	1.3	H_{α}	

the line-of-sight velocities is different on these two cuts. At the position angle $PA = 105^\circ$, the slit apparently goes outside the region where the emission of the gas belonging to the central subsystem dominates, and the line-of-sight velocity begins to increase, approaching 2100 km s^{-1} , the value that the subsystem of the galaxy's gaseous disk must have here. At $PA = 119^\circ$, the further decrease in the line-of-sight velocity with a smaller gradient ($30 \text{ km s}^{-1} \text{ kpc}^{-1}$) probably stems from the fact that the slit does not pass through the dynamic center of the decoupled subsystem.

The line-of-sight velocity curves at $PA = 60^\circ$ and $PA = 150^\circ$ are consistent with the assumption that a gaseous subsystem rotating around the major axis is present in the central part of the galaxy. At $R \leq 3''$, the curve also has a rectilinear segment with a gradient $dV/dR \approx 78 \text{ km s}^{-1} \text{ kpc}^{-1}$ northeast of the center at $PA = 60^\circ$ and with a gradient $dV/dR \approx 80 \text{ km s}^{-1} \text{ kpc}^{-1}$ at $PA = 150^\circ$. The outer segments of the line-of-sight velocity curves are determined by the galaxy's gaseous disk.

Thus, the behavior of all line-of-sight velocity curves indicates that there is a kinematically decoupled gaseous subsystem rotating around the major axis in the nuclear region of the galaxy. The change in the line-of-sight velocity gradient yields a preliminary estimate for the location of the dynamic axis of this gaseous subsystem ($PA \approx 110^\circ$). Its size is about $6''$ (1 kpc). At $R \geq 10''$, the line-of-sight velocity curves demonstrate the rotation of the galaxy's gaseous disk around its minor axis; the locations of the photometric axis on the periphery and the kinematic axis coincide and are close to $PA = 5^\circ$. An improvement of the kinematic features for the two gaseous subsystems based on 2D spectroscopy will be described below.

Our comparative analysis of the line intensities shows that the line intensity ratio $I_{[NII]\lambda 6583}/I_{H\alpha}$ does not exceed 0.4 everywhere, whence it follows that the emission is produced by photoionization. In this case, we can use the empirical method described by Denicolo et al. (2001) to determine the metallicity:

$$12 + \log(O/H) = 9.12(\pm 0.05) + 0.73(\pm 0.10) \times \log([SII]\lambda 6716 + [SII]\lambda 6731)/H_{\alpha} \quad (1)$$

As an example, Fig 3 shows the radial distributions of $12 + \log(O/H)$ for two cuts. An inner region ($r \leq 5''$) where this parameter is equal to ~ 8.6 and ~ 8.4 is distinguished in all distribution; farther out, it increases and reaches ~ 8.9 in outer regions. These values correspond to metallicities of $0.5Z_{\odot}$, $0.3Z_{\odot}$, and $0.9Z_{\odot}$, respectively. The spectrum along the galaxy's major axis ($PA = 5^\circ$) passes through the brightest condensations designated by Petrosyan (1981) as "b" and "c". In these regions, $12 + \log(O/H) \approx 8.6 \pm 0.1$ ($\sim 0.5Z_{\odot}$). The distribution constructed for $PA = 119^\circ$ (Fig. 3b) exhibits the lowest values, $12 + \log(O/H) = 8.4$ ($\sim 0.3Z_{\odot}$), at distances $R \leq 4''$ from the center. These region are located in the area of the kinematically decoupled gaseous subsystem, and the data for them apparently suggest that the metallicity of the central subsystem is slightly lower.

THE MORPHOLOGY OF NGC 7468

The IFP and MPFS intensity maps in the emission lines and in the continuum are shown in Fig. 4. The overall pattern of the brightness distributions in the red continuum and in the H_{α} line (Figs. 4a and 4b) demonstrates similarities, but numerous condensations of different sizes, which are probably HII regions, are distinguished more clearly in the H_{α} image. Chains of HII regions are observed on the southern side of the galaxy, and the southern lobe turns toward the brightening, where three bright condensations are distinguished. A lobe in the H_{α} brightness distribution and individual HII regions are also observed on the opposite side of the galaxy. Note that the HII regions in the central part of NGC 7468 form a ring of a roughly oval shape. This structure also shows up in the continuum brightness distribution, creating the illusion of a barlike structure (Taylor et al. 1994).

The galaxy's outer amorphous base has roughly elliptical isophotes with close axial ratios in the continuum ($b/a \approx 0.7$) and in the H_{α} line ($b/a \approx 0.65$); the geometrical center of the ellipses is $3''$ west of condensation "a". The lobes directed northward and southward are clearly seen in the continuum brightness distribution.

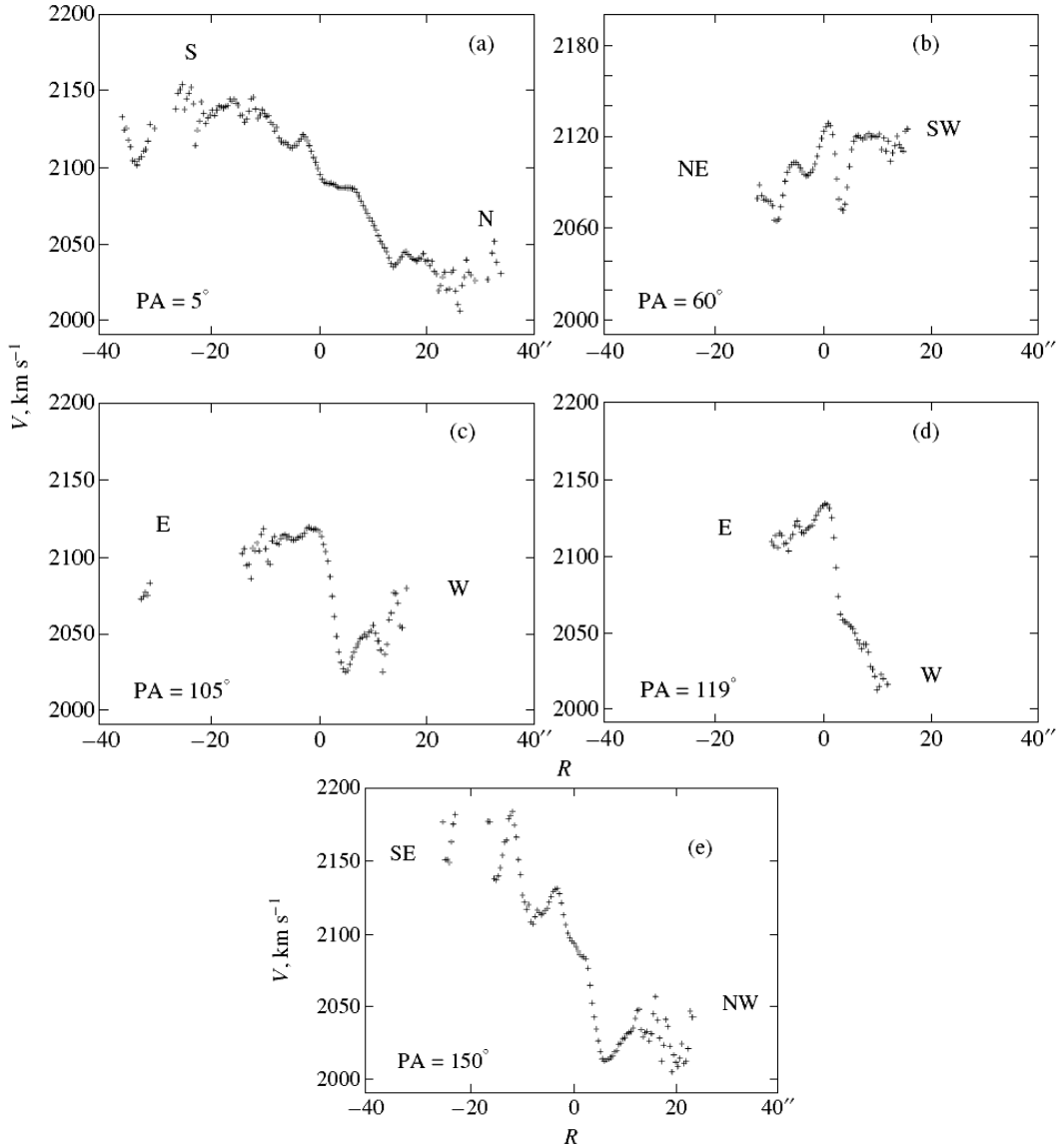


Fig. 2. NGC 7468: the UAGS line-of-sight velocity curves.

The three bright knots that correspond to condensations “a”, “b”, and “c” noted by Petrosyan et al. (1978) are clearly seen in the central part of the image in the green continuum (Fig. 4c). Condensation “c” is brightest. In the emission lines (Fig. 4), condensation “c” is poorly seen, while condensation “a” is most prominent. This characteristic feature was noted by Petrosyan (1981).

THE VELOCITY FIELDS OF THE IONIZED GAS AND STARS

Figure 5a shows the large-scale velocity field for the emitting gas, as constructed from the IFP data, suggesting the rotation of the galaxy’s gaseous disk around its minor axis. However, a feature indicating the rotation of the gas around the galaxy’s major axis is clearly seen in the central part of the velocity field. Thus, the IFP data confirm the presence of two kinematic subsystems of gas in this galaxy.

If the gas is assumed to rotate in circular orbits, then the method of “tilted-rings” can be used (Begeman 1989; Moiseev and Mustsevoi 2000) to analyze the velocity field. The method allows us to determine the positions of the kinematic center and the kinematic axis (the direction of the maximum velocity gradient), to estimate the galaxy’s inclination, and to construct the rotation curve. As we see from Fig. 6b, the location of the kinematic axis changes with increasing radius: $PA_{dyn} \approx 120^\circ$ in the nuclear region ($R \leq 6''$) and $PA_{dyn} \approx 180^\circ$ on the periphery. This confirms the existence of two kinematic subsystems of gas. The locations of the dynamic axes of the subsystems are close to those estimated from long-slit spectra. The subsystem associated with the central region is apparently the inner disk (ring) rotating around the galaxy’s major axis. The dynamic centers of the subsystems coincide, but are displaced by approximately $3''$ to the W of condensation “a”. The heliocentric line-of-sight velocity of the galaxy

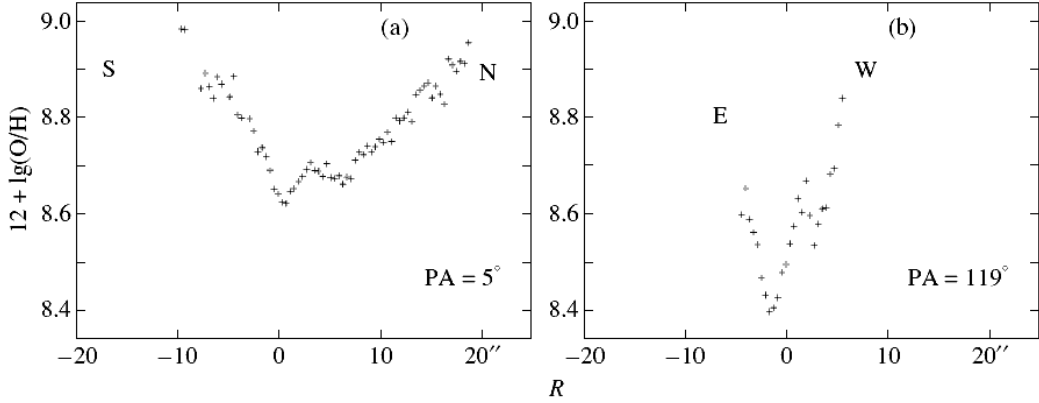


Fig. 3. Radial metallicity distributions.

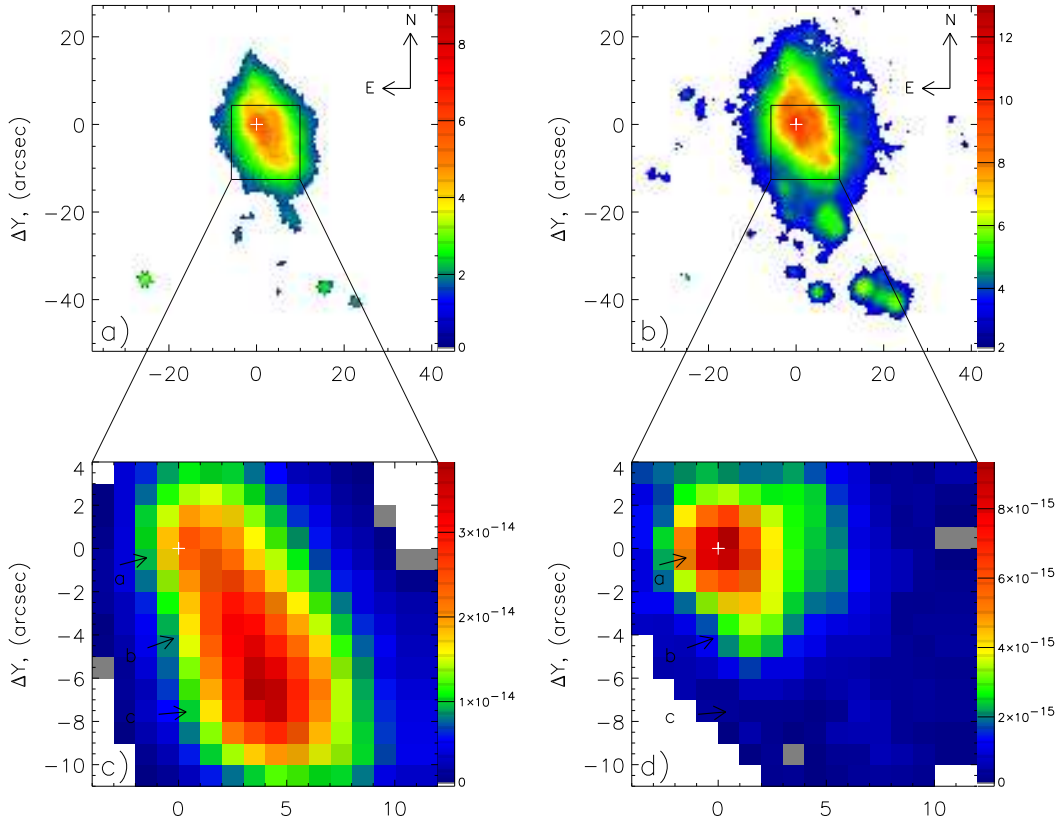


Fig. 4. IFP data: (a) images in the continuum near H_{α} ; (b) an image in H_{α} . MPFS data: the brightness distribution (c) in the continuum ($\lambda 5400 - 5500 \text{ \AA}$) and (d) in the $[\text{OIII}]\lambda 5007$ line. The gray scale corresponds to intensities in arbitrary units for panels (a) and (b) and to intensities in $\text{erg s}^{-1} \text{ cm}^2 \text{ arcsec}^{-2} \text{ \AA}^{-1}$ for panels (c) and (d). The pluses mark the position of the brightness maximum in the red continuum.

is $V_{sys} = 2070 \text{ km s}^{-1}$ or, after being corrected for the rotation of our Galaxy, $V_{gal} = 2220 \text{ km s}^{-1}$. The observed velocity field is best described by the model of circular rotation at an inclination of the galactic disk $i_{disk} \approx 45^\circ$ (which is equal to the estimate obtained from the galaxy's axial ratio) and that of the inner disk/ring, $i_{ring} \approx 60^\circ$. Here, two values of the angle between the galactic disk and the plane of the inner disk are possible: $\Delta i \approx 50^\circ$ and $\Delta i \approx 86^\circ$. In the first case, the orbits of the gas are unstable, and, therefore, noncircular motions must be observed

in the velocity field. However, such motions have not been found, so the second value (86°) of the angle between the galactic disk and the plane of the inner disk should be taken.

The observed rotation curve of the galaxy constructed from our data (crosses) and from the HI data of Taylor et al. (1994) (triangles) is shown in Fig. 6a. At $R \leq 3 \text{ kpc}$, the triangle lies well below the crosses. This is most likely because the 21-cm observations have a low spatial resolution ($\sim 3 \text{ kpc}$). At $R \geq 3 \text{ kpc}$, the discrepancy between

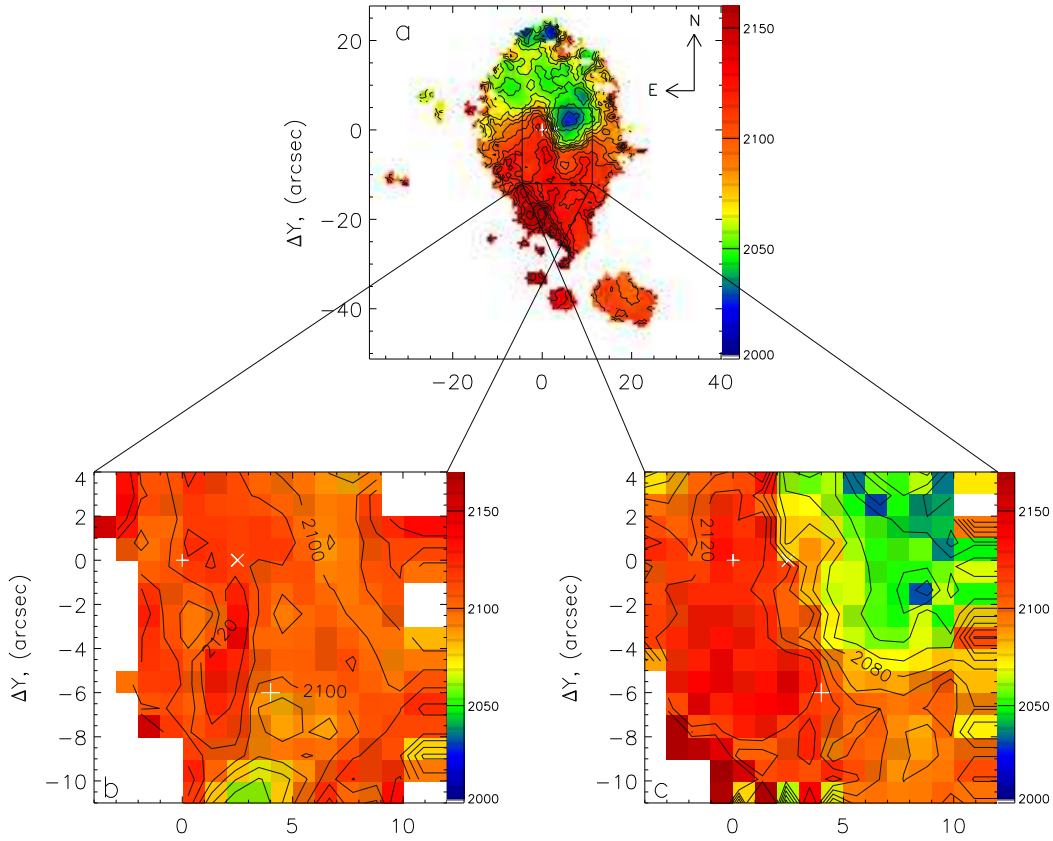


Fig. 5. (a) Large-scale velocity field, as inferred from IFP; (b) and (c) the velocity field of the stellar and gaseous components for the central region obtained from MPFS: the pluses indicate the positions of condensations “a” and “c” and the cross indicates the position of the dynamic center.

the optical and H I data decreases and does not exceed 10 km s^{-1} . The rotation curve reflects the motions in the inner disk/ring in the region $0 \leq R \leq 0.8 \text{ kpc}$ and the rotation of the galactic disk farther out. There is no significant jump in velocity when passing from one kinematic system to the other, which most likely suggests that the galaxy’s potential is spherically symmetric on these scales.

We analyzed the observed rotation curve using the models described by Monnet and Simien (1977). At distances of $0 - 3 \text{ kpc}$, it is well represented by an exponential disk model (the dashed line in Fig. 6a) with the scale factor $h = 0.9 \text{ kpc}$. This value is close to the estimates given by Evstigneeva (2000) and Cairos et al. (2001a), if these are recalculated to our assumed distance to the galaxy. Note that the photometric profile in the works by Evstigneeva (2000) was represented by two components: bulge+disk. However, our rotation curve does not confirm the presence of a bulge. If the galaxy actually had a bulge, then the velocity gradient in the central region would be much larger than that in our rotation curve. Therefore, we assume that the increase in brightness compared to the exponential law observed in the central part of the profiles could be due to the existence of regions of active star formation. The HI data show that the rotation curve flattens out somewhere at $8 - 10 \text{ kpc}$. Although there may be a small systematic shift between the optical and radio

data, in general, the run of the rotation curve at large distances from the center ($R \geq 3 \text{ kpc}$) can be explained by assuming the presence of an extended spherical isothermal halo. Its parameters were found to be the following: $r_c = 10 \text{ kpc}$, $\rho_0 = 0.002 M_\odot \text{ kpc}^{-3}$. The combined theoretical rotation curve is indicated in Fig. 6a by the solid line. The overall shape of the rotation curve is characteristic of late-type galaxies (Amram and Garrido 2002). The total mass of the galaxy, including the halo, is $2 \cdot 10^{10} M_\odot$, and the mass of the disk/ring assuming its radius to be 0.75 kpc is $\sim 4 \cdot 10^8 M_\odot$, or 2% of the galaxy’s mass.

The velocity fields for the stellar and gaseous components in the central part of the galaxy NGC 7468 are different (Figs. 5b and 5c). As we see from the figure, the ionized gas in this region rotates around the major axis, while the stellar velocity field is highly irregular. The velocity range does not exceed 40 km s^{-1} . The observed velocity variations can be explained by the presence of noncircular motions. It should also be noted that the contrast of the absorption features from the old stellar population is low for galaxies of late morphological types; therefore, the accuracy of the line-of-sight velocity measurements is lower than that of the usual MPFS observations of earlier-type galaxies, being $10 - 20 \text{ km s}^{-1}$. We attempted to describe the stellar velocity field using the method of “tilted-rings” with the fixed parameters PA and i corresponding to those

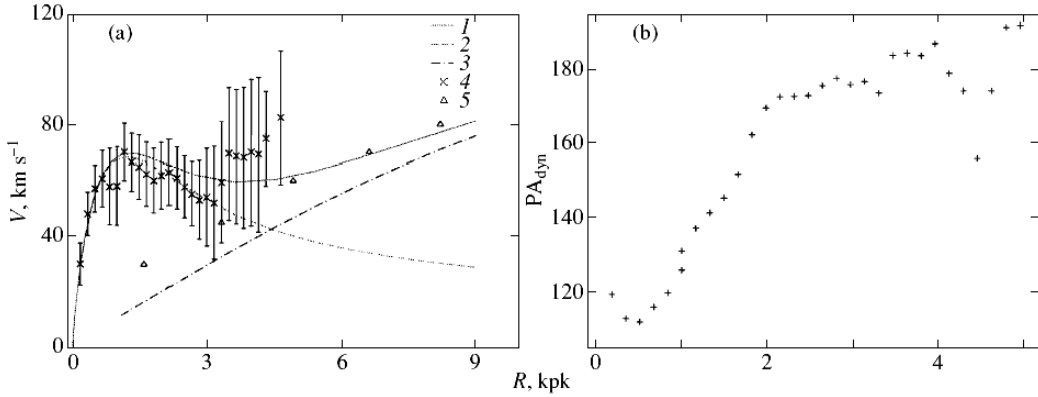


Fig. 6. (a) Rotation curves. 1: the resulting curve; 2: for the disk component; 3: for the halo; 4: our data; 5: the data from Richter et al. (1990). (b) The change in the location of the dynamic axis with radius.

of the galaxy's outer disk. The model describes the observations satisfactorily, except for the region near condensation "a", where large residual velocities ($\sim 50 \text{ km s}^{-1}$) are observed. We found no rotation around the major axis in the stellar velocity field. Therefore, we conclude that the stars and the gas in the galaxy's central region belong to different kinematic systems.

DISCUSSION

As was noted in the Introduction, the putative polar ring manifests itself in the galaxy's images as lobes on its northern and southern sides. However, analysis of the velocity field that we constructed from the IFP data and the velocity field derived from neutral hydrogen (Taylor et al. 1994) shows no peculiar features near these lobes. The gas in these regions is involved in the rotation of the galactic disk around the minor axis. Here, there is no kinematically decoupled subsystem characteristic of polar rings, which forces us to reject the assumption that NGC 7468 is a galaxy with an outer polar ring. The nature of the lobes and the brightening in the south is not quite clear. If we assume, following Taylor et al. (1993), that the galaxy to the north of NGC 7468 is spatially close to it (according to this paper, the difference between their line-of-sight velocities is 73 km s^{-1}), then these may be considered as tidal structures, as may be evidenced by the deviations of the observed velocities from the circular ones in the region of the brightening (by 40 km s^{-1}) and in the region of the southern lobe (by approximately 20 km s^{-1}). On the other hand, these may be weakly developed spiral arms. Their appearance and the color bluer than that for the remaining parts of the galaxy (Cairos et al. 2001b) can serve as evidence for this interpretation.

At the same time, we found a kinematically decoupled gaseous subsystem, a rotating inner disk, in the central part of NGC 7468 (~ 1.5 kpc in diameter). The angle between the galactic disk and the plane of the inner disk is 86° . Thus, we can assert that the galaxy has an inner polar disk (possibly, a ring) rather than a bar whose presence was used to explain some of the features in the velocity field constructed from the HI data (Taylor et al. 1994).

According to current views (Bournaud and Combes 2003), a polar structure in a galaxy can be formed either through accretion from a neighboring gas-rich galaxy during their close interaction or through the direct collision of galaxies, which can lead to the complete absorption of the less massive participant of the collision by the more massive galaxy. At the observed orientation of the inner disk, the position of the northern galaxy does not permit us to consider it a donor galaxy. Thus, we conclude that NGC 7468 collided with a low-mass gas-rich galaxy that was absorbed. As a result, a metal-poor polar gaseous disk was formed, and the observed induced star formation began in the central region of the galaxy (in a ring with a radius of $\sim 1.2 \text{ kpc}$). The individual condensations in this ring are spaced $0.5 - 1$ kpc apart. Such distances are observed between neighboring gas-dust clouds. The sizes of the condensations do not exceed 500 pc, in agreement with the sizes of stellar associations and stellar complexes. The intensity ratio of the emission lines suggests the photoionization mechanism of the emission in these regions.

Note also that the difference between the relative brightnesses of the condensations in the continuum and in the emission lines may be due to the age difference between these star-forming regions. Condensation "c", being relatively brighter in the continuum, may be an older stellar complex at a stage when the surrounding gas had already been partially swept up to large distances by strong light pressure light and/or supernova explosions.

CONCLUSIONS

Below, we summarize our results.

(1) Based on the long-slit spectra near H_α , we found a kinematically decoupled gaseous subsystem in the central region rotating around the galaxy's major axis.

(2) Our analysis of the line-of-sight velocity fields obtained using two-dimensional spectroscopy confirmed the existence of two kinematic subsystems of ionized gas: one of these is the gaseous disk of the galaxy, and the other is an inner disk 1.5 kpc in size. The angle between the planes of the disks is 86° ; i.e., the inner disk is polar. In

the central region of the galaxy, the stars and the ionized gas belong to different subsystems. (

3) The arc-shaped lobes on the northern and southern sides of the galaxy are not kinematically decoupled to an extent that the presence of the polar ring suggested by Whitmore et al. (1990) be confirmed. They are probably either tidal structures or weakly developed spiral arms.

(4) The intensity ratio of the forbidden and permitted lines confirms that the emission in HII regions results from photoionization. The derived metallicity is lower than the solar value ($\sim 0.3 Z_{\odot}$).

(5) The detected inner disk allows the galaxy NGC7468 to be classified as belonging to PRGs. The central collision with a dwarf galaxy and its capture could be responsible for the formation of the inner polar disk. The velocity field we derived shows that there is no reason to believe that the arc-shaped lobes on the northern and southern sides of the galaxy, which belong to the putative polar ring (Whitmore et al. 1990), are a kinematically decoupled ring. These are probably either tidal structures or weakly developed spiral arms.

Acknowledgements. We are grateful to the Large Telescopes Program Committee (LTPC) for allocating observational time on the 6-m telescope. This study was supported by the Russian Foundation for Basic Research (project nos. 02-02-16033 and 03-02-06766) and the Russian Ministry of Education (project no. E02- 11.0-5).

References

P. Amram and O. Garrido, 2002, astro-ph/0202475

V.L. Afanasiev, S.N. Dodonov, and A.V. Moiseev, 2001, Stellar Dynamics: from Classic to Modern, Ed. by L. P. Ossipkov and I. I. Nikiforov (Sobolev Astron. Inst., St. Petersburg), 103

K.G. Begeman, 1989, A&A, 223, 47

F. Bournaud and F. Combes, 2003, A&A, 401, 817

G. Denicolo, R. Terlevich, and E. Terlevich, 2001, MNRAS, 330, 69

E.A. Evstigneeva, 2000, Astrozika, 43, 519

L.M. Cairos, J.M. Vilchez, G. Perez, et al., 2001, ApJS, 133, 321

L.M. Cairos, N. Caon, J.M. Vilchez, et al., 2001, ApJS, 136, 393

A.V. Moiseev, 2002, Bull. SAO 54, 74 (astro-ph/0211104)

A.V. Moiseev and V. V. Mustsevoi, 2000, Astron. Lett. 26, 565 (astro-ph/0011225)

G. Monnet and F. Simien, 1977, A&A, 56, 173

T.E. Nordgren, G. Helou, J.N. Chengalur, et al., 1995, ApJS, 99, 461

A.R. Petrosyan, Astrozika, 1981, 17, 421

A.R. Petrosyan, K. A. Saakyan, and E. E. Khachikyan, 1979, Astrozika, 15, 209

O.R. Richter, P.D. Sackett, and L.S. Sparke, 1994, AJ, 107, 99

T.X. Thuan and G.E. Martin, 1981, ApJ, 247, 823

C. Taylor, E. Brinks, and E.D. Skillman, 1993, AJ, 105, 128

C.L. Taylor, E. Brinks, R.W. Pogge, and D. E. Skillman, 1994, AJ, 107, 971

B.C. Whitmore, R. A. Lucas, D. B. McElroy, et al., 1990, AJ, 100, 1489

T. Wiklind, F. Combes, and C. Henkel, 1995, A&A, 297, 643

W.K. Huchtmeier, L.G. Sage, and C. Henkel, 1995, A&A, 300, 675

L. V. Shalyapina, A. V. Moiseev, V.A. Yakovleva, et al., 2004, Astron. Lett., 30, 1 (astro-ph/0312564)

J.S. Young, S. Xie, J.D.P. Kenney, and W.L. Rice, 1989, ApJS, 70, 699

Translated by N. Samus'